IL NUOVO CIMENTO **39 C** (2016) 307
DOI 10.1393/ncc/i2016-16307-9

COLLOQUIA: SWGM 2015

The activation of non-linear optical response in Ag@ZnO nanocolloids under an external highly intense electric field

E. FAZIO([1])([*]), L. D'URSO([2]), S. SANTANGELO([3]), R. SAIJA([1]), G. COMPAGNINI([2]) and F. NERI([1])

([1]) *Dip.to di Scienze Matematiche e Informatiche, Scienze Fisiche e Scienze della Terra Università di Messina - Messina, Italy*
([2]) *Dip.to di Scienze Chimiche, Università di Catania - Catania, Italy*
([3]) *Dip.to di Ingegneria Civile, dell'Energia, dell'Ambiente e dei Materiali (DICEAM) Università Mediterranea - Reggio Calabria, Italy*

received 19 July 2016

Summary. — An extensive theoretical and experimental study of the non-linear optical properties of bare and silver-decorated zinc oxide (ZnO and Ag@ZnO) nanostructures, prepared by laser-generated plasmas in water and in water/polyvinyl alcohol (PVA) solutions, is reported. The z-scan technique was used to monitor the activation of the non-linear optical mechanisms, focusing an intense laser radiation through the nanocolloids under study. A classical formalism was adopted to explain the z-scan data of these anisotropic materials and to describe the influence of radiation torque and forces on the optically activated nanostructures. This modelling approach includes effects of nanoparticles rearrangements, also taking into account plasmonic effects. An interesting coupling between the nature of the optical limiting response and the nanostructures reorganization under the high-power laser excitation, used during the z-scan measurements, was found and, for the first time to our knowledge, was explained using a classical theoretical approach.

1. – Introduction

Wide band gap semiconductors have been recently the object of extensive studies because of the rising interest in the development of new non-linear optical (NLO) materials for potential applications in integrated optics, namely applications of second harmonic generation in wave guides and in ultraviolet photonic devices as well.

([*]) Corresponding author. E-mail: enfazio@unime.it

Among the investigated materials, nanostructured ZnO thin films have gathered considerable attention because of their large non-linearity conjugated with good piezoelectric characteristics, high-energy conversion efficiency, photoluminescence enhancement, and efficient UV lasing [1]. On the other hand, the excellent UV shielding effects observed in ZnO-based polymeric nanocomposites, such as ZnO/polystyrene and ZnO/polystyrene-polymethylmethacrylate films, offer wide prospects of applications as efficient UV-protection coatings [2].

Nanoparticles (NPs) of noble metals, such as Ag, Au, or Cu, embedded in dielectric matrices have been widely investigated because of their large third-order NLO susceptibility and fast response time, which are essential requirements for future optical device applications, such as optical switches, optical phase conjugation and optical computing [3]. The great enhancement of optical non-linearity in the metal-semiconductor nanocomposite materials generally stems from the giant amplification of the local electric field near and inside the metal particles at the surface plasmon resonance frequency, in the visible region [4].

A limited number of studies is reported in the literature for hybrid metal/ZnO aqueous nanocolloids, chemically and morphologically stable, with a narrow size distribution, showing a significant NLO response as well. Krishnan *et al.* [5] reported excellent third-order non-linearity on stable ZnO colloids prepared by chemical method in the presence of capping agents while Irimpan *et al.* [6] reported self-defocusing non-linearity and good non-linear absorption behaviour (two photon absorption followed by free carrier absorption mechanism), which increases with increasing Ag volume fraction. However, to our knowledge, no systematic study regarding the correlation between the NLO response of these systems and the effect of the external highly intense electric field (as the ones in the z-scan focal region) on the morphological and optical properties of the ZnO-based NPs, prepared in different liquid environment, is reported in the literature.

In this work, the effect of water or PVA/water solution, in which nanostructures are generated, is investigated giving particular emphasis on the change of the NPs surface electrostatic charge that the liquid environment induces and on the different NLO-activation mechanisms. A positive charge characterized the NPs surface of the PVA/water Ag@ZnO colloid while all the other samples show a negative charge. Even for this same sample, the highest NLO absorption contribution is estimated. On the overall, an interesting coupling between the nature of the optical limiting response and the NPs rearrangement under a high-power laser excitation was found, explaining the z-scan data by a classical approach able to account for the effects of the "NPs asymmetry"/rearrangement and plasmonic effects.

2. – Experimental section

2˙1. *Sample preparation.* – The second harmonic (532 nm) of a laser operating at 100 kHz repetition rate with a pulse width of 6 ps was used for the ablation experiments. The laser beam was focused to a spot of about 70 μm in diameter on the surface of the target with a Galvanometric scanner having a telecentric objective with a length of 163 mm. Silver and metallic zinc targets of 3 mm thickness (99.99% purity) were positioned on a holder within a glass vessel and separately ablated at a laser power density of 1.5 J cm^{-2} in distilled water or in aqueous PVA solution. The PVA/water solution was obtained by dissolving 7.5 gr of PVA (average molecular weight: 86000) in 30 mL of distilled water. The dispersion was heated to the temperature of 90 °C, subsequently left to reflux under magnetic agitation for 2 h, and finally cooled down to room temperature

(RT). The dispersion was further diluted in water to obtain a 7.5% P/V final solution. Ablation in water was performed for 16 min. In the case of PVA/water solution 16 ablation processes of 1 min duration were carried out, spaced out by 10 min for thermalisation purposes. Ag@ZnO nanocolloids were obtained by mixing ZnO and Ag colloidal solutions, in 1:1 volume ratio, immediately after their production. After preparation, all the solutions were stirred at RT in an ultrasonic bath for about 15 min.

2˙2. *Sample characterisation.* – Samples morphology was investigated by the use of a JEOL TEM 2010 F electron microscope operating at an accelerating voltage of 200 kV. Selected-area electron diffraction (SAED) patterns were recorded to study the crystallographic structures of the samples. The zeta potential of the samples was quantified using a nanoparticles analyzer operating in the range between 0.3 nm and 8 μm, using a Horiba dynamic light scattering (DLS) setup. UV-vis optical transmission measurements were carried out on a Perkin-Elmer Lambda 750 spectrophotometer. The UV-vis optical transmission of the as-prepared colloidal solution was measured in the 190–600 nm range both immediately after the ablation process and at end of NLO limiting measurements. The NLO properties were determined by the z-scan method [7] using a pulsed Nd:YAG laser (532 nm wavelength, 5 ns pulse duration, 10 Hz repetition rate). As shown in appendix A, a beam-splitter divided the incident laser beam (fig. 7); a first detector collected the reflected portion (input), while a 300 mm lens focused the transmitted one (output) into a 1 cm length quartz cuvette. A second detector, mounted at 90° with respect to the laser propagation direction, allowed collecting simultaneously the scattered light (point-to-point along z) with a dual channel energy meter. The optical limiting measurements were carried out by moving the sample along the axis of the incident beam (*i.e.* z-direction) with respect to the focal point while keeping constant the laser pulse energy (fig. 7). To determine the non-linear refractive index n_2, the non-linear absorption coefficient β and the 90° scattering efficiency S, the measurements were taken in both open and closed aperture configurations [12]. In the closed aperture configuration a finite aperture ($d = 500\,\mu$m) was placed at 300 mm from the focal point. All measurements were carried out with a laser fluency of 1.5 J cm^{-2} in the focal region (see also appendix A).

3. – Results

3˙1. *TEM and DLS analyses.* – Figure 1 shows the morphology of the samples, as resulting from high-resolution transmission electron microscopy (HRTEM) analyses. A relatively uniform distribution of nearly spherical NPs, smaller than 50 nm in diameter, is observed for zinc oxide (fig. 1(a)) and silver (fig. 1(b)). In the case of the Ag@ZnO hybrid nanostructues prepared in water (fig. 1(c)), Ag NPs (rounded darker features) result to be embedded within the oxide matrix. Some core-shell nanostructures are observed in the case of Ag@ZnO nanocomposites prepared in PVA/water (fig. 1(d)). The outer shell is constituted by PVA macromolecules. The inner core consists of ZnO agglomerates (dashed yellow circle) or Ag NPs (dashed red circle) with different size, 50–100 nm for the former and about 25 nm for the latter.

The study of the crystallographic structure of the samples by means of SAED reveals the polycrystalline nature of the ZnO, consisting of randomly oriented grains (inset of fig. 1(c)). Electron diffraction patterns relative to Ag@ZnO hybrids prepared in water (inset of fig. 1(c)) are better defined than those relative to samples prepared in PVA/water (not shown). The coexistence of rings with different intensity and definition is indicative of the presence of randomly oriented nano-sized ZnO particles.

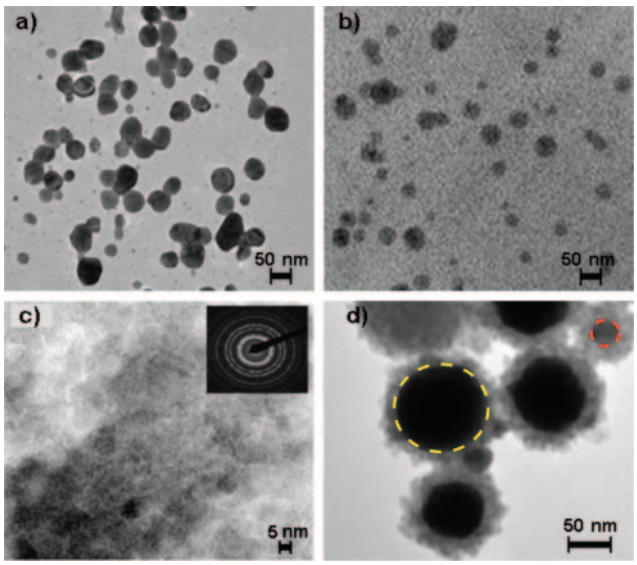

Fig. 1. – TEM micrographs of (a) ZnO, (b) Ag NPs, and of Ag@ZnO hybrids in (c) water and in (d) PVA/water. Inset to image (c): SAED pattern of Ag@ZnO hybrids in water, where the (100), (101), (102), (112), (103), (002) and (201) rings are visible.

TABLE I. – *Zeta potential values obtained by DLS measurements.*

Ablation medium	Samples	Zeta potential (mV)
Water	ZnO	−7.1
	Ag	−22.0
	Ag@ZnO	−13.6
PVA/water	ZnO	−5.3
	Ag	−11.5
	Ag@ZnO	9.6

Being a measure of the electrostatic potential that exists on the NPs surface, DLS data provide information regarding the surface charge and stability of the nanoparticulate formulation. In the presence of Ag NPs, the ZnO nanostructures prepared in water show a slightly more negative value (table I), indicating that the mixing with metal NPs reduces the electrophoretic mobility and partly stabilises the oxide ones against aggregation, as useful for long-term storage. In the aqueous PVA solution, the stability of Ag and ZnO suspension is ascribed to steric/electrostatic stabilization promoted by the large molecules of polymer PVA. Thus, the partial shielding of the NPs surface charges masks their negative charge. Otherwise, the potential of Ag@ZnO prepared in PVA/water shifts towards a positive value (+9.6 mV). PVA coating results in relatively stable Ag@ZnO colloids with a modified surface charge, in a manner similar to the case of colloidal silica nanoparticles [8]. Such an occurrence is possibly due to the rearrangement of the overall colloidal structure, that will be related to peculiar NLO response, as we outline in the following section.

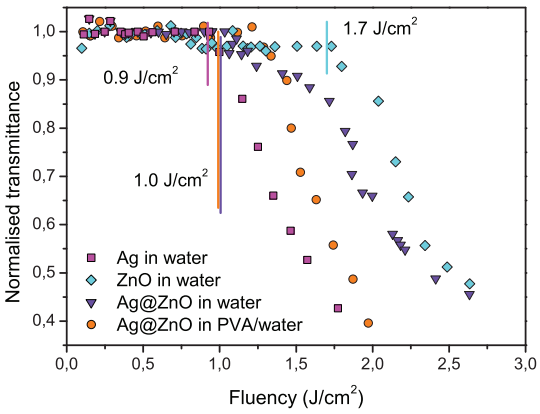

Fig. 2. – NLO limiting performance of the nanocolloids toward the 532 nm laser light input.

3˙2. *Z-scan data analysis*. – Figure 2 displays limiting curves relative to the hybrid Ag@ZnO nanocolloids and their separate components (Ag and ZnO). Transmittance T is calculated as (point-to-point along z) ratio between output and input beam intensities. Then, the so-obtained values are normalised to the ones acquired out of the region of non-linearity. Normalised transmittance begins to decrease at a fluency of 0.9, 1.0 and 1.7 J cm^{-2} for Ag, Ag@ZnO and ZnO samples, respectively. Transmittance is halved at 2 J cm^{-2} for ZnO and Ag@ZnO colloids in water; for Ag and Ag@ZnO colloids in PVA/water, transmittance reaches nearly 1/2 of the initial value at about 1.5 J cm^{-2}. No NLO response is observed for both water and PVA/water solutions (not shown). Only after several repeated cycles of measurements, a softening of the optical limiting response is observed, even if the effect is still active.

In order to determine the nature of non-linear mechanisms, z-scan measurements were carried out both in the open and closed aperture configurations, by respectively measuring the real and imaginary part of the third-order susceptibility (χ^3) [7]. Hence, the normalised transmittance curves, reported as a function of the z-scan position and analysed using the procedure proposed by Bahae *et al.* [9] described in appendix A, allow to distinguish the pure non-linear absorption contribution from the refractive one. For this purpose, the refractive contribution to the non-linearity is isolated from the absorption contribution by dividing normalised transmittance T_{closed}, collected along the beam direction propagation with a pinhole placed before the detector (closed configuration), by the normalised transmittance T_{open} without any aperture (open configuration).

Figure 3 displays transmittance and scattering values as a function of the sample position z. In ZnO and Ag@ZnO samples prepared in water, the T_{open} signal (fig. 3(a)) is characterised by a symmetrical increase, peaking near the position ($z = 0$), while the S signal (fig. 3(b)) decreases in the focus region. Thus, the S contribution affects the T increase and, ultimately, the NLO response of the samples. Moreover, the peak-to-valley configuration of fig. 3(c) indicates a negative change of the refractive index (self-defocusing effect), as expected for most of the dispersive materials [10]. Colloids prepared in PVA/water are characterised by a T_{open} curve (fig. 3(d)) with a symmetrical minimum in the focus region and no change in the 90° scattering signal (fig. 3(e)). This behaviour implies that the optical limiting response is mainly determined by the non-linear absorption mechanism. $T_{\text{closed}}/T_{\text{open}}$ ratios of the PVA/water samples are similar

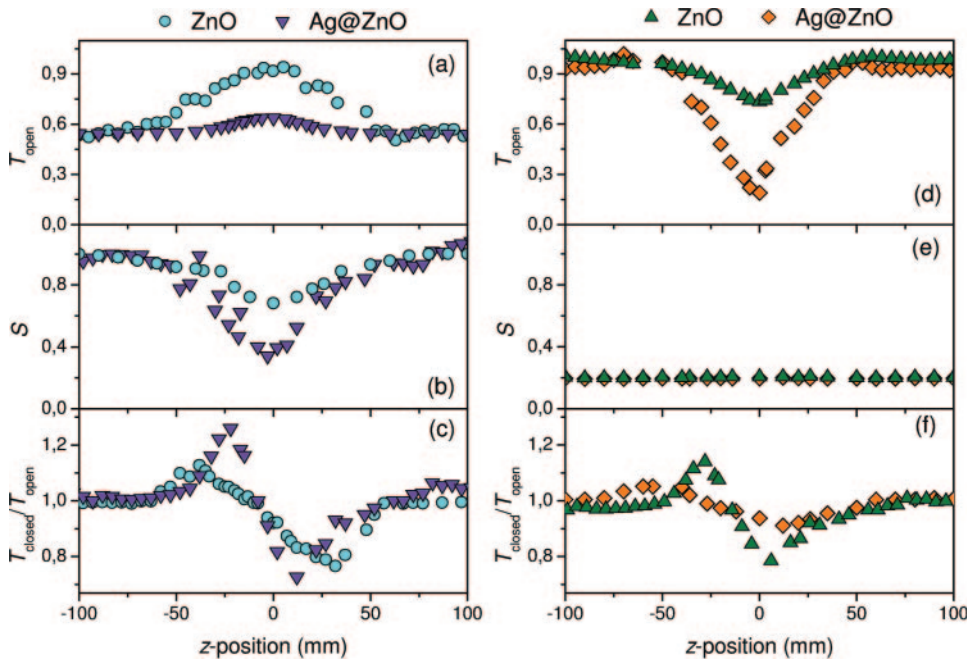

Fig. 3. – (a), (d) Transmittance $T_{\rm open}$, (b), (e) 90° scattering S, and (c), (f) transmittance ratio $T_{\rm closed}/T_{\rm open}$ as a function of the sample position z. Plots (a)–(c) and (d)–(f) refer to samples prepared in water and PVA/water solution, respectively.

to that observed in water (compare figs. 3(f) and 3(c)), even if signals relative to ZnO and Ag@ZnO samples are closer in the case of PVA/water than in the case of water. Since, as mentioned above, no signal is collected if the z-scan measurement is carried out on the PVA/water solution (*i.e.* in the absence of the ZnO and Ag NPs), the observed limiting effect is an intrinsic property of the hybrid Ag@ZnO colloids.

Keeping fixed the ZnO concentration, the Ag NPs are added to the ZnO water colloids. Also in this case, two different behaviours are observed in water and in water/PVA together with an improvement of NLO response. In water, the scattering signal decreases in the focus region, showing a dip that reaches a minimum value around 0.2, while the signal collected along the beam propagation direction (open configuration) is characterized by a slight increased transmittance symmetrical peak near the focus position. Then, as in the case without Ag NPs, the reduced scattering contribution affects the NLO response of the water Ag@ZnO colloids. In water/PVA, the open transmittance curve of the Ag@ZnO colloids shows a remarkable symmetrical minimum in the focus region. This behavior implies that the mechanism which mainly determines the optical limiting response is the nonlinear absorption mechanism (the dip is a feature characteristic of a Reverse Saturable Absorption mechanism). No change in the 90° scattering signal was detected. Thus, the contributions associated with the variation of the scattering effects are not relevant to determine the nonlinear optical response.

Non-linear absorption coefficient β and non-linear refraction index n_2 values can be quantitatively evaluated from normalised open transmittance and from difference between peak and valley transmittance ΔT_{p-v} in the closed/open curves,

TABLE II. – *Results of z-scan fitting procedure.*

Sample	β (cm GW^{-1})	n_2 (10^{-17} m^2 W^{-1})	α (cm^{-1})
ZnO in water	−8.3	−2.1	2.25
Ag in water	65.2	−1.9	0.36
Ag@ZnO in water	−78.3	−2.8	1.43
ZnO in PVA/water	22.8	−2.4	0.16
Ag in PVA/water	83.1	−0.9	0.05
Ag@ZnO in PVA/water	197	−2.2	0.11

respectively [11, 12]. The results obtained by this procedure are reported in table II. All the samples show comparable values of the nonlinear scattering signal S and of the nonlinear refractive index n_2. However, although S and n_2 remain almost unchanged, the β value is significantly high and with an opposite sign for the Ag@ZnO in PVA/water with respect to the Ag@ZnO in water.

An explanation of the reasons which determined the different NLO mechanisms is difficult to provide with the only z-scan data. In our opinion, the interpretation of NLO response is of "microscopic" origin and it could be due to the mechanical effects induced by the high power laser excitation on the Ag-connected ZnO NPs.

In this contest, by a classical theoretical approach and taking into account the information obtained simulating the UV-vis linear optical absorption response (next section), we investigate the effect of a focused highly intense electric field on the NPs dynamics which, in turn, reflects on the NLO absorption and scattering mechanisms.

3˙3. *UV-vis optical absorbance analysis.* – Figure 4(a) compares the experimental (continuous lines) and computed (dashed lines) UV-vis absorption spectra of the Ag colloidal solutions obtained in water and PVA/water. A theoretical approach based on the multipole expansion of the electromagnetic fields and the transition matrix method [13] was here followed to reproduce and analyse the UV-vis absorption spectra of Ag and ZnO colloids. This approach allowed indirectly to estimate the size of the colloids and the PVA shell thickness. All this information will be used to reproduce the z-scan data.

The correlation between the UV-vis resonance peak location and the NPs size is obtained performing the simulations on bare Ag spherical NPs, calculating the extinction

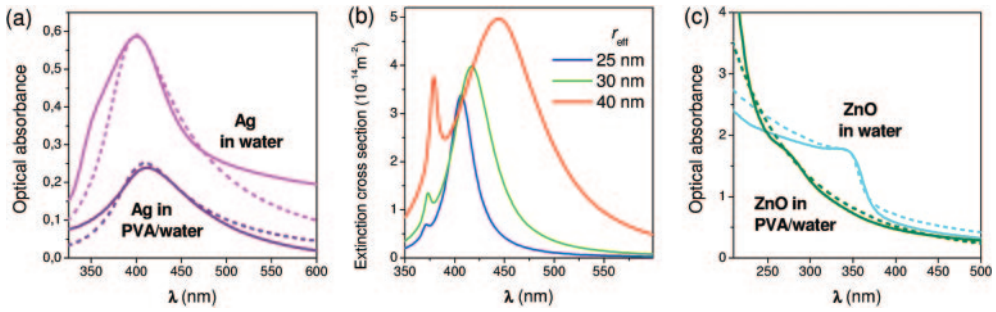

Fig. 4. – (a), (c) Experimental (continuous lines) and theoretical (dashed lines) optical absorbance spectra of (a) Ag and (c) ZnO NPs, and (b) computed extinction cross-sections, plotted in arbitrary units, for Ag nanospheres with different radius.

cross-section C_{ext} in the dilute concentration limit. The optical constants for silver in the simulations are those measured by Johnson *et al.* [14]. To ensure the convergence in the multipole expansion, we considered the longitudinal fields and dielectric function, as introduced by Lindhard [15] and simplified by Pack *et al.* [16]. We took into account the meaningful wavelength dependence of the real part of water dielectric constant, while neglecting the dependence on wavelength of the imaginary part [17]. The resonance peak location was addressed to silver NPs with effective radius r_{eff} of 25 nm.

The presence of PVA in water induces a change in the optical properties of the sample. The main changes in the optical absorbance spectrum are:

– a non-negligible decrease of plasmon resonance intensity;

– a noticeable red shift of the Surface Plasmon Resonance (SPR) wavelength (from 400 nm up to 410 nm).

The two modifications indicate that the sizes of the particles grown in the PVA/water solution are not greater than those found in water. In fact, the computed cross-sections for nanospheres different in size (fig. 4(b)) reveal that the red shift of the plasmon resonance due to an increase in the NPs size also leads to an increase of the intensity. Hence, the decrease in intensity observed in our case suggests that the observed optical absorption features are ascribable to the modification of the environment for the presence of PVA. In particular, the peculiar optical absorbance of Ag@PVA solution was determined considering a core-shell nanostructure in water, with the core formed by a bare Ag spherical NPs having $r_{\text{eff}} = 25$ nm, coated by a 15 nm thick PVA-shell. The optical constants of PVA in the simulations are those reported in ref. [18].

Figure 4(c) compares the experimental and computed UV-vis absorption spectra of the ZnO colloids obtained in water and PVA/water solution. A size distribution with $r_{\text{eff}} = 10$ nm was here considered to simulate the optical absorbance of ZnO in water [19]. Analogously to what emerged from a previous study on ZnO ablated NPs [20], the departure of the experimental absorbance from the theoretical one in the range 200–340 nm, below the absorption edge, is indicative of the presence of aggregates. Differently, the presence of PVA induces a dramatic blue-shift of the ZnO optical absorption edge feature, resulting in its nearly complete disappearance. This points out that smaller particles surrounded by PVA macromolecules were formed. By the best fit procedure, we have found that the core is formed by a bare ZnO spherical NPs with $r_{\text{eff}} = 4$ nm, and the PVA-shell has a thickness of 30 nm. The optical constants of ZnO used are those obtained by spectroscopic ellipsometry for epitaxial ZnO thin layer [21].

4. – Discussion

Ag and ZnO nanocolloids were prepared by pulsed laser ablation in water and in PVA/water environment. Samples characterizations in terms of optical and morphological properties indicate the synthesis of spherical Ag@ZnO aqueous nanocolloids with a narrow size distribution. We have found a surface charge positive sign and a high NLO absorption coefficient value for the PVA prepared Ag@ZnO colloids. On the contrary, the other investigated samples show negative values of the NPs surface charge as well as a different nature of the NLO optical response. In this case, a NLO scattering mechanism dominates with respect to the other ones (two-photon absorption followed by weak free carrier absorption, inter-band absorption and local density refractive index change).

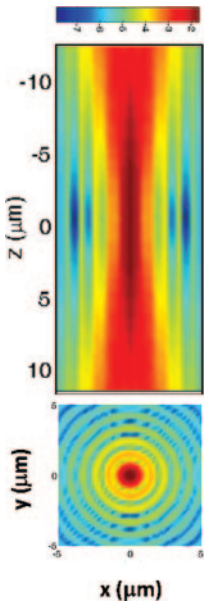

Fig. 5. – Map of the incident field in focal region, as calculated by means of the angular spectrum representation.

As mentioned in the previous paragraphs, despite the z-scan measurements showed totally different behaviors in water and PVA, the explanation of what has been observed is difficult to give. Thus, to reproduce z-scan behaviours, the main assumptions are that pronounced photoinduced NPs aggregation and reorientation take place at higher energy density (focal region). However, this occurrence happens only when the NPs are asymmetrical. Therefore, since the NPs shape is mainly spherical as shown by SEM images, the only plausible explanation is that the NPs asymmetry manifests itself, in the colloidal phase, under the action of an intense electric field.

In the following, before discussing about our simulated results, we report some useful information to understand the adopted theoretical approach. From the theoretical point of view, the transmittance measured through a z-scan experiment is the result of the interaction of a focused electromagnetic field (EMF) with the NPs immersed in the liquid environment [12, 22, 23]. Considering the optical system typical of the z-scan experiments (see appendix A), we assume that the optical axis coincides with the z-axis of a rectangular coordinate system, and the nominal focus F of the lens is located at the origin O. The back focal plane is illuminated by an unpolarised TEM_{00} Gaussian beam propagating in water ($n_0 = 1.33$) along the positive direction of the z-axis, with filling factor 2 and wavelength $\lambda_0 = 530\,\text{nm}$. The numerical aperture of the lens in water is NA = 0.22. The map of the incident field in the focal region is calculated by means of the angular spectrum representation [24, 25]. Figure 5 shows the distribution of the field intensity on a logarithmic scale. Despite having overlooked the aberrations due to the air/glass transition, we can observe how broad the focal region is in the z direction and how the variation of the intensity in the transverse plane is relevant.

It is well known that, in the interaction between the EMF and the matter, light exerts a mechanical action on NPs. Hence, starting from the conservation of linear and angular momentum of the whole field/nanostructure system, the formalism that we devised to

describe the mechanical effects on single and aggregated particles makes full use of the Maxwell stress tensor [26], in which the fields are the superposition of the field incident on the particles and of the field scattered by the particles themselves. Accordingly, both these fields are expanded in a series of vector spherical multipole fields [27], in terms of which amplitudes all the quantities of interest are given. The multipole amplitudes of the scattered field are calculated from those of the incident field through the transition matrix approach [28] that applies to particles of any shape, even of high aspect ratio, and resorts to the only approximation of truncating the series to an order sufficient to ensure convergence.

The basic interaction of light with an anisotropic particle is the same as the one with a spherical particle, and the force can be calculated using the formula:

$$\mathbf{F}_{\mathrm{rad}} = \oint_S \hat{\mathbf{n}} \cdot \langle T_M \rangle \mathrm{d}S, \tag{1}$$

where the integration is carried out over a surface S surrounding the scattering particle, $\mathbf{n}$ is the surface outer normal unit vector, and $\langle T_M \rangle$ is the averaged Maxwell stress tensor, which describes the mechanical interaction of light with matter. In terms of the incident/scattered EMF we get

$$\mathbf{F}_{\mathrm{rad}} = -\frac{\epsilon r^2}{4} \int_\Omega \left[|\mathbf{E}_s|^2 + \frac{c^2}{n^2} |\mathbf{B}_s|^2 + 2\Re \left\{ \mathbf{E}_i \cdot \mathbf{E}_j^* + \frac{c^2}{n^2} \mathbf{B}_i \cdot \mathbf{B}_s^* \right\} \right] \hat{\mathbf{r}} \mathrm{d}\Omega. \tag{2}$$

If the particle is non-homogeneous or has a geometrical asymmetry, two major differences arise in field/matter interaction with respect to spherical particles. The first one is that in the case of non-spherical objects a significant torque can also appear. The radiation torque due to a monochromatic EMF can be calculated as

$$\Gamma_{\mathrm{Rad}} = -r'^3 \int_{\Omega'} \hat{\mathbf{r}}' \cdot \langle T_M \rangle \times \hat{\mathbf{r}}' \mathrm{d}\Omega', \tag{3}$$

in terms of total EMF

$$\Gamma_{\mathrm{rad}} = -\frac{\epsilon r^3}{2} \Re \left\{ \int_\Omega \left[(\hat{\mathbf{r}} \cdot \mathbf{E})(\mathbf{E}^* \times \hat{\mathbf{r}}) + \frac{c^2}{n^2} (\hat{\mathbf{r}} \cdot \mathbf{B})(\mathbf{B}^* \times \hat{\mathbf{r}}) \right] \mathrm{d}\Omega \right\}. \tag{4}$$

This torque tends to align the elongated/asymmetric particle along the optical axis.

The second difference is that, for a spherical particle, the radiation pressure is always directed in the propagation direction because of symmetry; while for anisotropic shapes, the radiation pressure, even in the case of a plane wave, has a transverse component that is responsible for the optical lift effect, *i.e.*, non-spherical particles can move transversely with respect to the incident light propagation direction [29, 30]. Generally, the presence of the non-uniform field in the focal region, where there is a strong intensity gradient, facilitates the aggregation of the nanostructures, induces the alignment of the asymmetrical particles, and for high numerical aperture lens (NA > 0.9) causes also the trapping [31-34].

Thus, since in our experiment the lens has a moderate numerical aperture, we believe that the most relevant effect is the gradual alignment of the asymmetric NPs that, under the effect of radiation pressure, pass through the focal region. They align in the two

possible orientations: 1) parallel to the optical axis, or 2) in the polarisation plane of the electromagnetic fields [32].

Figures 6(a), (b) show the variation of the normalised (longitudinal and transversal) cross-sections for ZnO and Ag@ZnO structures dispersed in water with tilt angle θ_z. The normalisation is performed through the ratio between the cluster cross-section and the total cross-section of the monomers constituting the aggregate. When $\hat{k}_s||\hat{k}_i$, the quantity $\sigma_{\mathrm{rad},||z}$ is the extinction cross-section averaged on $\theta_{x,y}$ as a function of the θ_z tilt angle. On the other hand, when $\hat{k}_s \perp \hat{k}_i$, $\sigma_{\mathrm{rad},\perp z}$ is the scattering cross-section averaged on $\theta_{x,y}$, computed along the y direction (see geometry in fig. 6).

Taking into account the UV-vis analysis, z-scan profiles are simulated considering, in water, NPs aggregates of ZnO monomers with $r_{\mathrm{eff}} = 10\,\mathrm{nm}$ and Ag NPs with $r_{\mathrm{eff}} = 25\,\mathrm{nm}$, as well as for different geometrical morphology of the aggregates, obtained through a random number generator. As a first approach, varying proportions of Ag and ZnO were considered. The z-scan data were well reproduced when linear clusters with $\gamma = 6$

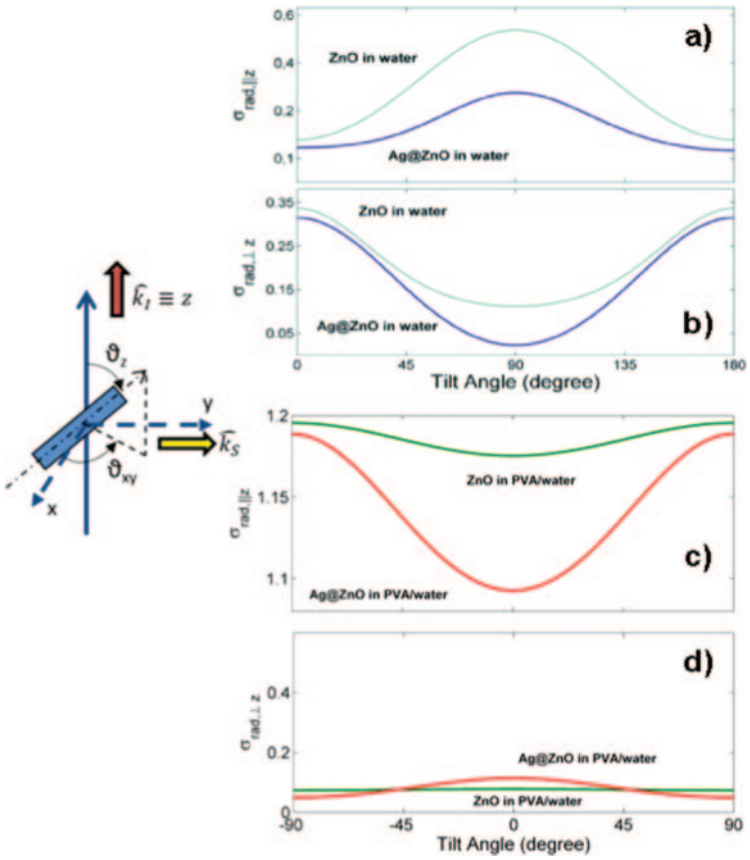

Fig. 6. – Normalised cross-sections for asymmetric nanostructures featured by the aspect ratio parameter γ. Plots (a) and (b) show the variation of cross-sections as a function of the tilt angle, θ_z (see geometrical sketch on the left of the plots). The data shown refer to clusters with $\gamma = 6$. Plots (c) and (d) show the variation of cross-sections as a function of the tilt angle, θ_z, considering clusters with $\gamma > 10$.

and an equal number of monomers of ZnO and Ag are considered (see figs. 6(a), (b)). In figs. 6(a), (b), the cyan curves refer to clusters built by means of the aggregation of solely ZnO NPs, instead the violet ones refer to cluster composed by Ag and ZnO NPs. We notice that the maximum in extinction (fig. 6(a)) corresponds to the case where the cluster shows a preferential orientation along the polarization plane. Simultaneously, a minimum in the differential scattering cross-section computed in the perpendicular plane to $\hat{k}_i$ is found. For the water Ag@ZnO hybrid colloids, behaviours analogous to the ones observed for the only ZnO were found. In this case, the reduced transmittance/scattering signal can be ascribed to the presence of Ag NPs interposed between the ZnO nanoaggregates.

The z-scan profiles of the samples prepared in PVA/water are simulated considering the formation of ZnO nanostructures with $\gamma > 10$. These ZnO nanoaggregates are mainly composed of monomers with a r_{eff} of 4 nm, coated by a 30 nm PVA shell. Similarly, we considered Ag NPs with r_{eff} of 25 nm (as in the case in water) but surrounded by a PVA shell of 15 nm.

Figures 6(c), (d) show the variations of the normalised cross-sections for PVA/water ZnO and Ag@ZnO colloids. We notice that the minimum in extinction (fig. 6(c)) corresponds to the case of cluster with orientation parallel to the optical axis ($\theta_z = 0°$). This gives a differential scattering cross-section in the direction perpendicular to $\hat{k}_i$, which does not substantially depend on the angular variation. In good agreement with experimental z-scan profiles, in PVA the scattering signal is not observed either for the ZnO NPs or for the Ag@ZnO nanosystems.

In conclusion, the interplay between the different mobility of uncoated and coated NPs and the induced guiding action of the electric field results in a dynamical behaviour different for the NPs dispersed in water and PVA. In water, the high mobility of the asymmetric nanostructures with low γ ($= 6$) favours their alignment on the polarization plane without a preferential orientation. This is due to the interaction between the electric field and the dipole momentum of the nanostructures. In PVA, the reduced efficiency of the dipole momentum of the coated Ag NPs and the high γ value (> 10) of the hybrid system cause a significant radiation torque that induces an alignment along the optical axis.

5. – Conclusion

An extensive theoretical and experimental study of NLO properties of ZnO and Ag@ZnO nanostructures, prepared by laser-generated plasmas in water and in PVA/water solutions, is reported. A theoretical approach based on multipole expansion of the electromagnetic fields and the transition matrix method is adopted to reproduce the UV-vis optical absorption spectra of the investigated samples and also to explain the activated non-linear mechanisms, experimentally collected carrying out z-scan measurements. In particular, the influence of radiation torque and forces on the optically activated nanostructures response is outlined. This modelling approach takes into account NPs orientation, alignment and aggregation. An interesting coupling between the nature of the optical limiting response and the nanostructures alignment under the high-power laser excitation, used during the z-scan measurements, is found. Given the good results obtained for zinc oxide nanoparticles, the proposed method deserves an extension to other colloidal systems in order to check for a more general applicability.

Appendix A.

NLO analysis

In nonlinear optics a z-scan measurement is used to measure the non-linear index n_2 (Kerr nonlinearity) and the non-linear absorption coefficient β via the "closed" and "open" methods, respectively. As the non-linear index can affect the measurement of the non-linear absorption, the open method is typically used in conjunction with the closed method. The equipment is arranged as can be seen in fig. 7. A lens focuses a laser to a certain point, and after this point the beam naturally defocuses. After a further distance an aperture is placed with a detector behind it. The aperture causes only the central region of the cone of light to reach the detector. In the scattering configuration, the detector is placed at 90° with respect to the optical axis and it moves together the quartz cuvette placed onto a translation stage.

The estimation of the nonlinear absorption coeffcient β and the refractive one can be carried out using the following procedure. When the aperture (S) is removed before the detector, the z-scan transmittance is insensitive to the beam distortion, and it is only a function of the nonlinear absorption. The total transmitted power $P(z,t)$ is given by

$$P(z,t) = P_i(t)\exp^{-\alpha L}\frac{I[1+q_0(z,t)]}{q_0(z,t)},$$

where $\alpha(I)$ includes linear and nonlinear absorption terms; L is the sample length; and $q_0(z,t)$ is the parameter characterizing the strength of the nonlinearity given by the following expression:

$$q_0(z,t) = (\beta I_0(t))\frac{L_{\text{eff}}}{1+z^2/z_0^2},$$

where z is the sample position; L_{eff} is the effective interaction length; z_0 is the Rayleigh diffraction length; $P_i(t)$ is the instantaneous input power defined as

$$P_i(t) = \frac{\pi\omega_0^2 I_0(t)}{2}$$

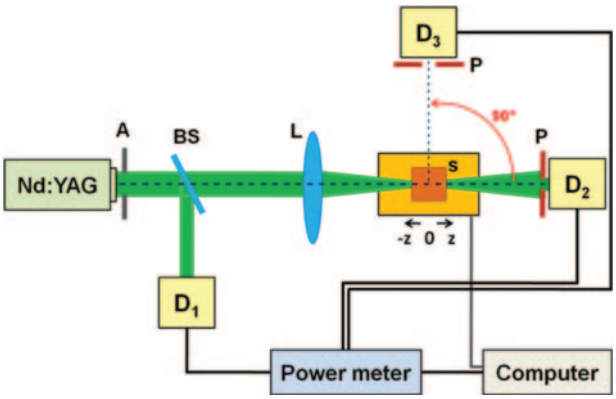

Fig. 7. – Scheme of the z-scan measurement.

and S is the aperture linear trasmittance given by

$$S = 1 - \exp(-2r_a^2/\omega_0^2),$$

with r_a denoting the beam radius at the aperture, in the linear regime. For a temporally Gaussian pulse, the normalized energy transmittance is expressed by

$$T(z, S = 1) = \frac{1}{\sqrt{\pi} q_0(z, 0)} \int_{-\infty}^{+\infty} I[1 + q_0(z, 0) \exp(-i\tau^2)] \mathrm{d}\tau.$$

Moreover, for $|q_0| < 1$, this transmittance can be expressed in terms of the peak irradiance in a summation, more suitable for numerical evaluation:

$$T(z, S = 1) = \sum_{m=0}^{\infty} \frac{[-q_0(z, 0)]^m}{(m + 1)^{3/2}}.$$

Thus, for $S = 1$, fitting experimental data with this expression, the nonlinear absorption coefficient β was unambiguously deduced. With β known, the z-scan with aperture $S < 1$ can be used to determine the coefficient n_2. In this case, the closed/open z-scan transmittance can be reproduced considering a geometry-independent normalized transmittance as

$$T(z) \propto 1 - \frac{4x}{(x^2 + 9)(x^2 + 1)},$$

where $x = z/z_0$, while the peak and valley transmittance values are calculated by solving the equation $\mathrm{d}T(z)/\mathrm{d}z = 0$. Thus, the nonlinear refraction index n_2 value can be estimated using the relation

$$n_2 = \frac{\lambda}{2\pi L} \frac{\Delta T_{p-v}}{0.406(1 - S)^{1/4} I},$$

where λ is the laser wavelength, and S is the finite aperture parameter. Finally, knowing β, the nonlinear scattering coefficient α was estimated taking into account that the transmitted intensity through the sample is given by

$$\frac{\mathrm{d}I}{\mathrm{d}z} = -\alpha - \beta I^2.$$

Appendix B.

UV-vis absorbance analysis

Unlike the chemical approaches, adopting the pulsed laser ablation in liquid (PLAL), the amount of the prepared products cannot be estimated directly by weighing. The PLAL technique consists in the mass removal by coupling laser energy to a target material. When the laser radiation is focused on the surface of a solid target, pulsed-laser radiation can be absorbed through various energy transfer mechanisms, leading to thermal and non-thermal heating, melting, and finally ablation of the target. Laser ablation is one of the most efficient physical methods for micro-, and more recently, nanofabrication, due to the high resolution capability, low heat deposition in the target and high

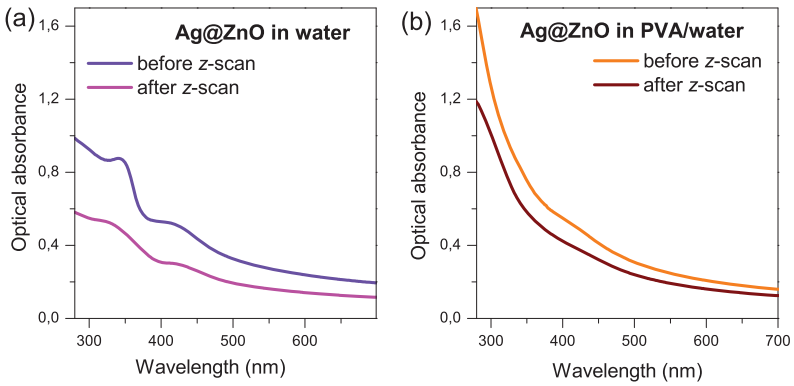

Fig. 8. – Optical absorbance spectra of the Ag@ZnO nanocolloids in water (a) and in PVA/water (b) before and after z-scan measurements.

level of flexibility. The ablation of the target yields an ejection of its constituents and the formation of nanoclusters and nanostructures which, when the target is ablated in liquids, are dispersed in the solvent.

Therefore, the silver amount in the water solution was indirectly calculated by analyzing UV-vis spectra and taking into account microscopy results. The concentration of the Ag nanocolloids was indirectly calculated from the plasmon resonance position, taking into account NPs size estimated by TEM, using the method proposed by Link and El Sayed [35].

On the overall, the estimated concentration of the Ag colloid in water and in PVA are about $5 \cdot 10^{-5}$ M and 10^{-6} M, assuming an average molar extinction coefficient of $2.5 \cdot 10^4\,\mathrm{M^{-1}cm^{-1}}$. In the dilute concentration limit, from the absorbance measurements at the absorption edge, we determine the concentration c of ZnO nanoparticles, following the relation

$$A = (\hat{C}_{\mathrm{ext}} N l)/2.303,$$

where C_{ext} is the extinction cross-section corresponding to the r_{eff} of the dispersion, l is the optical path length. The calculated concentration is $c = 2 \cdot 10^{-4}\,\mathrm{gr/cm^3}$.

Figure 8 shows the UV-vis optical absorbance spectra before and after z-scan measurements. Both the characteristic surface plasmon resonance (SPR) of the Ag NPs, above 400 nm, and the absorption edge of ZnO, below 400 nm, are almost unchanged after the measurements, indicating that no degradation of the colloidal solutions occurs. This proves the good photo-stability of the samples.

REFERENCES

[1] Lee G. J., Lee Y. P., Jung S. G., Hwangbo C. K., Kim S. and Park I., *J. Appl. Phys.*, **102** (2007) 073528.
[2] Tu Y., Zhou L., Jin Y. Z., Gao C., Ye Z. Z., Yang Y. F. and Wang Park Q. L., *J. Mater. Chem.*, **20** (2010) 1594.
[3] Cotter D., Manning R. J., Blow K. J., Ellis A. D., Kelly A. E., Nesset D., Phillips I. D., Poustic A. J. and Rogers D. C., *Science*, **286** (1999) 1523.
[4] Ricard D., Roussignol P. and Flytzanis C., *Opt. Lett.*, **10** (1985) 511.
[5] Krishnan B., Irimpan L., Nampoor V. P. N. and Kumar V., *Physica E*, **40** (2008) 2787.

[6] Irimpan L., Nampooril V. P. N. and Radhakrishnan P., *Chem. Phys. Lett.*, **455** (2008) 265.
[7] Fazio E., Neri F., Patanè S., D'Urso L. and Compagnini G., *Carbon*, **49** (2011) 306.
[8] Kim K.-M., Kim H. M., Lee W.-J., Lee C.-W., Kim T., Lee J.-K., Jeong J., Paek S.-M. and Oh J.-M., *Int J. Nanomedicine*, **9** (2014) 29.
[9] Sheik-Bahae M., Said A. A., Wei T., Hagan D. J. and Van Stryland E. W., *IEEE J. Quantum Electron.*, **26** (1990) 760.
[10] Messina E., D'Urso L., Fazio E., Satriano C., Donato M. G., D'Andrea C., Maragò O. M., Gucciardi P. G., Compagnini G. and Neri F., *J. Quant. Spectros. Radiat. Transfer*, **113** (2012) 2490.
[11] Fazio E., Patanè S., D'Urso L., Compagnini G. and Neri F., *Opt. Commun.*, **285** (2012) 2942.
[12] Fazio E., D'Urso L., Consiglio G., Giuffrida A., Compagnini G., Puglisi O., Patanè S., Neri F. and Forte G., *J. Phys. Chem. C*, **118** (2014) 28812.
[13] Borghese F., Denti P. and Saija R., *Scattering from Model Nonspherical Particles* (Springer, Berlin) 2007, Chapt. 4, pp. 73–106.
[14] Johnson P. B. and Christy R. W., *Phys. Rev. B*, **6** (1972) 4370.
[15] Lindhard J., *Mat.-Fys. Medd. K. Dan. Vidensk. Selsk.*, **28** (1954) 8.
[16] Pack A., Hietschold M. and Wannemacher R., *Opt. Commun.*, **194** (2001) 277.
[17] Segelstein D. J., M. S. thesis, University of Missouri-Kansas City (1981).
[18] Hamad K. T., *J. Al-Nahrain Univ.*, **16** (2013) 164.
[19] Mishchenko M. I., Hovenier J. W. and Travis L. D., *Light Scattering by Nonspherical Particles: Theory, Measurements, and Applications* (Academic Press, New York) 1999, Chapt. 6, pp. 147–170.
[20] Fazio E., Cacciola A., Mezzasalma A. M., Mondio G., Neri F. and Saija R., *J. Quant. Spectros. Radiat. Transfer*, **124** (2013) 86.
[21] Postava K., Sueki H., Aoyama M., Yamaguchi T., Ino Ch., Igasaki Y. and Horie M., *J. Appl. Phys.*, **87** (2000) 7820.
[22] Fazio E. and Neri F., *Appl. Surf. Sci.*, **272** (2013) 88.
[23] Forte G., D'Urso L., Fazio E., Patanè S., Neri F., Puglisi O. and Compagnini G., *Appl. Surf. Sci.*, **272** (2013) 76.
[24] Novotny L. and Hecht B., *Principles of Nano-Optics* (Cambridge University Press) 2008, Chapt. 2, pp. 38–42.
[25] Neves A. A. R., Fontes A., Padilha L. A., Rodriguez E., Cruz C. H., Barbosa L. C. and Cesar C. L., *Opt. Lett.*, **31** (2006) 2477.
[26] Jackson J. D., *Classical Electrodynamics* (Wiley, New York) 1975, Chapt. 10, pp. 456–506.
[27] Rose E. M., *Elementary Theory of Angular Momentum* (Wiley, New York) 1956, Chapt. 7, pp. 127–131.
[28] Waterman P. C., *Phys. Rev. D*, **3** (1971) 825.
[29] Saija R., Iatì M. A., Giusto A. and Borghese F., *J. Quant. Spectros. Radiat. Transfer*, **2** (2005) 163.
[30] Swartzlander A. G. jr., Peterson T. J., Artusio-Glimpse A. B. and Raisanen A. D., *Nat. Photon.*, **5** (2011) 48.
[31] Saija R., Denti P. and Borghese F., *Optical Force and Torque on Single and Aggregated Spheres: The Trapping Issue* (Springer) 2012, Chapt. 6, pp. 157–192.
[32] Messina E., Donato M. G., Zimbone M., Iatì M. A., Calcagno L., Fragalà M. E., Compagnini G., D'andrea C., Foti A., Gucciardi P. G. and Maragò O. M., *Opt. Express*, **23** (2015) 8720.
[33] Jones P. H., Palmisano F., Bonaccorso F., Gucciardi P. G., Calogero G., Ferrari A. C. and Maragò O. M., *ACS Nano*, **3** (2009) 3077.
[34] Borghese F., Denti P., Saija R., Iatì M. A. and Maragò O. M., *Phys. Rev. Lett.*, **100** (2008) 163903.
[35] Link S. and El-Sayed M. A., *J. Phys. Chem. B*, **103** (1999) 8410.